

International Journal of Multidisciplinary Research and Growth Evaluation.



Microstructure characteristics and mechanical properties of ductile iron at varied copper addition and section thickness

Kutelu BJ 1*, Ogundeji FO 2, Oluyori RT 3

- ¹⁻² Department of Mineral and Petroleum Engineering Technology. The Federal Polytechnic, Ado-Ekiti, Ekiti, State, Nigeria
- ³ Department of Metallurgical and Materials Engineering, Kogi State Polytechnic, Lokoja, Nigeria
- * Corresponding Author: Kutelu BJ

Article Info

ISSN (online): 2582-7138

Volume: 05 Issue: 04

July-August 2024 **Received:** 15-04-2024; **Accepted:** 13-05-2024

Page No: 61-68

Abstract

Performance integrity of ductile cast iron (DCI) has been enhanced by different metallurgical approaches. Consequently, in this study, conjoint influence of varied weight percent of copper and section thickness on DCI properties was investigated. The control and 0.05 wt%., 0.35 wt% and 0.85 wt.% of copper alloyed samples were produced using a definite sized rectangular wooden greensand mould and cylindrical wooden pattern with 10 mm, 30 mm and 85 mm section thickness. Optical emission spectrometry (AR 4 30 metal analyzer) was used to determine chemical compositions of the samples and the corresponding carbon equivalent values (CEVs) were calculate using the expression [($CE = \%C + \frac{1}{3}\%(Si + P)$]. Metallurgical microscope (model number NJF-120A) was used to examine the samples' microstructures. Standard test specimens for tensile, hardness and impact were prepared following ASTM E8, ASTM E 8-04 and ASTM A370 respectively, and the specimens were tested using standard equipment. From the results, the control and copper alloyed samples were comprised silicon as the major element, while the other elements were presnt in trace quantities. Microstructures of all the samples were characterized by spheroidal graphite, which were relatively homogeneously distributed in pearliticferritic matrix, and also visible were graphite nodule of different sizes and spacing. In addition, traces of carbide in relative amounts were present in microstructures of the alloyed samples. Generally, for all section thickness, tensile (UTS and YS) and hardness properties of the alloyed samples were improved over the control samples, while inverse was the case for ductility. Impact energy characteristic of the control samples was high relative to the alloyed samples. Hence, the resulting DCI samples offer better performance under low to medium loading conditions than high loading condition.

Keywords: greensand, microstructures, spheroidal graphite, pearlitic-ferritic, nodule counts and nodularity

1. Introduction

Ductile iron (DI) is a family of cast iron whose microstructure is characterized by graphite nodules in pearlitic-ferritic matrix, the nodules are formed by addition of nodulizers such as magnesium, yttrium or cerium into the melt (Collin-Garua *et al.*, 2020; Allan, 2012) [10,1]. DI is known with better strength and ductility relative to grey cast iron (GCI), and has exceptional combination of good toughness, wear and corrosion resistance, and shows impressive performance at elevated temperature. These properties coupled with its low cost of manufacturing comparable compacted cast iron (CCI) and steel endeared its use for a wide range of applications in construction industry (Bahubali and Vasudev, 2013) [6].

It is used in automobile construction, including highway diesel trucks, class 8 trucks, agricultural tractors, fully machined piston for large marine diesel engine, bevel wheel, hydraulic clutch on diesel engine for heavy vehicle and fittings, exhaust manifold, wheel hubs, crankshaft, camshaft, heavy duty diesel engine, intake manifold, thyrod automotive components, wheels, gear boxes,

oil well pump, overhead electric transmission line (Allan, 2012; Dwight, 1943) ^[1]. DI is also used for pipes, pump housing, bollards and industrial machinery such as wind turbine electrical energy generation, valves, air conditioning machinery and lawn (Krawiec *et al.*, 2006).

Mechanical properties/austemperity of DI have been improved by alloy additions. Copper is a strong pearlite promoter, during eutectic transformation, copper coarsens graphite and stabilizes pearlite, increases graphitization potential, and increases the number of eutectic cells, while reducing eutectic cell size (Gorny and Iyrala, 2012; Tsuijikaiva, (2011) [13, 20], and improved hardness and strength of DI to the raising pearlite to ferrite ratio that resulted from copper addition (Das et al., 2013) [11]. Nodule count and nodularity, and pearlite fraction and melting temperature (TM) of the DI are influenced by solidification conditions of the melt. For a given cooling rate, nodule count increases, while pearlite fraction decreases, and with increased cooling rate, increased pearlite fraction is increased (Haji and Husse, 2017) [14]. Melting temperature (TM) of DI increases with increasing solidification time, the higher the

solidification time, the lower the nodule formed and the risk of microstructural defects, including micro shrinkage, graphite degeneration and high segregation become high increased (Gorny and Iyrala, 2012) [13]. Also, the more the graphite shape deviates from the ideal spherical shape, the lower are the mechanical properties of the DI in application under varying loading conditions (Valek *et al.*, 2012) [41]. Consequently, efforts made in this study were aimed at utilizing these metallurgical routes (alloying and solidification conditions) at achieving optimum mechanical properties through adequate combination of copper addition

2. Materials and Method

and section thickness.

2.1. Materials

Chemical composition of the auto part (engine block) scrap used for the work as obtained by optical emission spectrometry (AR 4 30 metal analyzer) is depicted in Table 1. Other materials used were graphite, copper wire, ferrosilicon, limestone and nodulizer.

Table 1: Elemental composition of scrap from auto parts

%C 3.97	%Si 1.94	%Mn 0.87	%P 0.088	%S 0.131	%Cr 0.163	%Ni 0.058	%Mo 0.0015
%Al 0.0058	%Cu 0.137	%Co 0.015	%Ti 0.0015	%Nb <0.0025	%V 0.0099	%W <0.010	%Pb 0.0083
%Mg 0.0033	%B <0.0005	%Sn 0.0083	%Zn 0.0081	% As 0.020	%Bi <0.0015	%Ce <0.0030	%Zr <0.0015
%La <0.0033	%Fe 92.5						

2.2 Method

2.2.1Mould preparation

Greensand was mixed with bentonite and coal dust in the presence of appropriate amount of water. Was added to mixture. Wooden rectangular pattern of length 50 mm and breadth 30 mm with section thicknesses of 10 mm, 30 mm and 85 mm were used. Adequate allowances for shrinkage, machining, draft, rapping and distortion were ensured. Parting sand was sprinkled on a moulding board, drag and the patterns were placed on the moulding board. Facing sand was riddled around the pattern and rammed properly using hand rammer until it was completely covered. And the drag was filled with backing sand and rammed to compact. The drag was turned over carefully, parting sand and embargo was sprinkled over it. Thereafter, cope was placed over the drag and aligned properly using pins. The gating system (sprue, and gates, and risers) were arranged accordingly, and facing sand was added up to one-third of the cope and rammed, backing sand was then added to fill the cope and rammed to compact. A funnel-shaped impression meant for pouring was cut on top of the sprue passage and vent wire was used to create holes in the mould for easy passage of any trapped air or gases. After which, the cope was separated from the drag and dressed, and the risers and the pattern were carefully removed from the drag, air was blown into it to remove excess sand particles. The mould cavity and other passages were coated with graphite coat, the mould was n pre-heated by firing. Afterwards, the cope was assembled on the drag and some loads were placed on top of the assembly to apply pressure for support against melt pressure when pouring.

2.2.2. Casting of samples

A 50Kg capacity rotary furnace was used for melting the scrap, prior charging the scrap was shattered into pieces with

sledge hammer to allow for free passage through the charging sprout of the furnace, thereby protecting the furnace lining from eroding. The graphite was broken into smaller sizes with the aid of a sledge hammar, while the limestone was pulverized using pestle and mortar. Other charges, including varied amount of copper (0.05% wt., 0.85% wt., and 1.35% wt), nodulizer (0.2g magnesium), fluxing agent (lime) and inoculant (FeSi - 78% Si, 0.21% Al, Fe-bal) with particle size 1.2 mm were prepared in the required amounts. And in order to achieve uniform melting rate. the furnace was preheated for 60 to 70 minutes. Afterwards, the furnace was charged and heated to high temperature, optical pyrometer used to monitor the temperature at regular interval. The charge weight of each melt was 30Kg, and at1,470oC, the charges have melted. The inoculant was added to the metal stream when tapping to ladle at 1,470oC (Harvey and Noble, 2007; Skjegstad and Skaland, 1996), and the liquid metal was given adequate time to gradually transform into a solid cast at the room temperature (23oC) in the mould. This was necessary to avoid any hot shaking effects on the solid state solidification (Choi et al., 2004). After which, the castings were knocked out. Procedure for producing the different batches of castings is shown in Table 2.

Table 2: Summary of the casting procedure

Batch No.	Section thickness (mm)	Copper addition (wt.%)
1	10, 30 and 85	Nil
2	10, 30 and 85	0.85
3	10, 30 and 85	1.35

2.3. Chemical compositions and carbon equivalent of the samples

Optical emission spectrometry (AR 4 30 metal analyzer) was used to obtain chemical composition of ductile cast irons. And carbon equivalent of the sample CE of the ductile cast

irons was determined using the expression in Eqn. 1 (Harvey and, Noble, 2007).

$$CE = \%C + \frac{1}{3} \%(Si + P)$$
 (1)

2.4. Microstructure examinations

Specimens of the unalloyed and copper alloyed ductile cast iron from each of the section thickness were prepared for optical microscopic examination. The specimens were ground on a water lubricated silicon carbide abrasive papers of 180, 240, 320, 400 and 600 grit sizes. Polishing was carried out on 15cm rotating discs of a POLIMET universal polishing machine with synthetic velvet polishing clothes impregnated with 1 μm Alumina paste. The specimens were then etched with 2% nital solution using the swabbing method with cotton wool soaked in the etchant and then rinsed with water. The metallogahic samples were prepared based on ASTM E3-11

(2011). The microscopic examination was carried out using a Metallurgical microscope (model number NJF-120A) to obtain the different microstructures of the grey cast iron. An image analyzer (image J) was used to measure and obtain precise values of nodule count, nodularity, volume fraction of ferrite and pearlite, and carbide phases present in each of the sample

2.5. Mechanical testing

2.5.1. Tensile test

The tensile test samples were machined to standard dimensions as specified in ASTM E8-08.(2008) (Fig. 1). The test method adopted was ASTM E8. The test sample was mounted at its ends onto the holding grips of the testing apparatus. Each sample was subjected to tension till fracture, after which tensile strength and percentage elongation were taken.

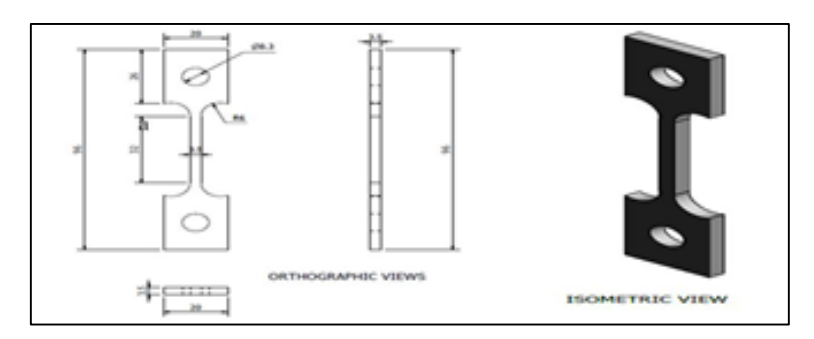


Fig 1: Tensile test specimen

2.5.2 Hardness test

Hardness specimens with dimension 20 mm length, 20 mm breadth and 4.5 mm thickness (Fig.2) were prepared in accordance with ASTM E384-11 (2011) standard. Universal Rockwell hardness tester model 8187LKV was used. The specimen was placed on the anvil and moved up until it came

in contact with the diamond cone indenter, the dial gauge was set to zero using minor load of 10kgf. Thereafter, major load of 150kgf was applied on the specimen, and the corresponding hardness value was measured on the C-scale. Three indentations were made with gap of about 3 mm inbetween and the average values were recorded.

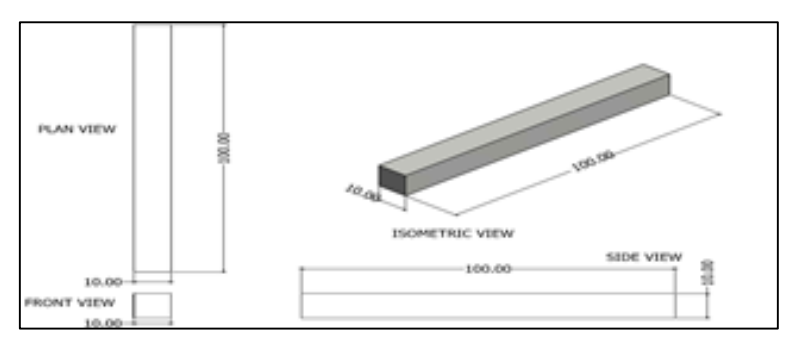


Fig 2: Hardness test specimen

2.5.3 Impact test

The impact test samples were machined to standard dimensions of length 10 mm, breadth 10 mm and height 55 mm with a depth of 1 mm V-notch at 45° (Fig. 3) based on

ASTM A370. (2008). The test specimen was gripped horizontally in a vice, and the trigger was then released. The energy absorbed in Joules in breaking the specimen was registered by pointer of the quadrant scale and recorded.

Fig 3: Impact test specimen

3. Results and Discussion

${\bf 3.1}$ Chemical compositions and carbon equivalent of the samples

The control and copper alloyed samples are comprised majorly of silicon and other elements (Table 2). The high silicon and low manganese contents of the samples may have been set to increase graphitization and avoid segregation respectively, and the presence of nickel was necessary to improve mechanical properties of the castings (Das *et al.*,

2013) ^[11]. From Table 3, it is indicative that the DI samples are hyper-eutectic (Collin-Garua *et al.*, 2020; Harvey and. Noble, 2007) ^[10]. And increased ferrite phase and nodule count of the control sample with corresponding decreased nodularity relative to the copper alloyed samples resulted from increased silicon content of the former (Das *et al.*, 2013) ^[11], and the increased CEV of the alloyed samples with increasing copper addition agreed with the findings the past researchers (Allan, 2012; Tsuijikaiva, 2011) ^[1,20].

Table 2: Chemical compositions of the samples

	Description of Sample					
Element	Control	0.05wt. % Cu	0.85wt. %. Cu	1.35%wt.% Cu		
С	3.410	3.812	3.846	3.885		
Si	2.394	2.148	2.364	2.401		
Mn	0.433	0.486	0.412	0.411		
P	0.032	0.039	0.040	0.015		
S	0.023	0.019	0.012	0.009		
Al	0.123	0.126	0.122	0.126		
Mg	0.068	0.049	0.033	0.047		
Cu	0.165	0.462	0.517	0.672		
Sb	0.001	0.003	0.004	0.003		
Ni	0.031	0.028	0.024	0.014		
Mo	0.019	0.006	0.004	0.003		
Cr	0.076	0.052	0.071	0.075		
V	0.011	0.013	0.005	0.002		
Fe						

Table 3: Copper equivalent values of the samples

S/No	wt. %Cu	CEVs
1.	0.00	4.191
2.	0.05	4.541
3.	0.85	4.635
4.	1.35	4.688

3.2 Microstructure

3.2.1 Microstructure characteristics of the control sample at varied section thickness

Microstructures of the control, unetched samples with section thickness of 10 mm, 30 mm and 85 mm Plates 1 (a-c) are comprised of homogeneously distributed spheroidal graphite

in pearlitic-ferritic matrix, and microstructures of the corresponding etched samples are characterized by graphite nodule of different sizes and spacing in pearlitic-ferritic matrix (Tsuijikaiva, 2011) [20]. The small regions of segregation revealed by the sample with 10 mm section thickness relative to samples with 30 mm section thickness and 85 mm section thickness respectively, was accounted for by increased cooling rate (Haji and Husse, 2017) [14], and variations in volume fraction of ferrite, pearlite and carbide phases of the samples was due to difference in cooling rates (Gorny and Iyrala, 2012; Behnam *et al.*, 2010) [13, 7].

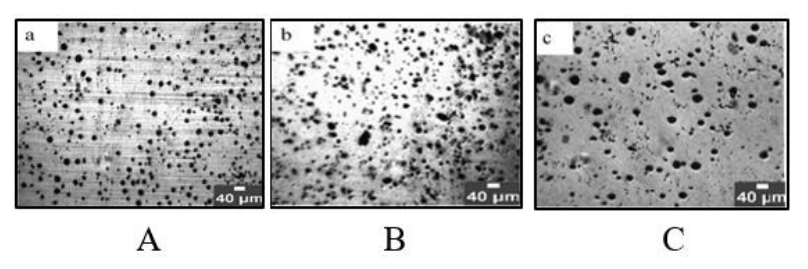


Plate 1: (a-c). Microstructures of the control ductile iron with section thickness (a) 10mm, (b) 35mm and (c) 85 mm respectively

Plate 2: (a-c). Microstructures of etched control ductile iron with section thickness (a) 10mm, (b) 35mm and (c) 85mm respectively etched in 3% Nital solution

3.3.2. Microstructure characteristics of copper alloyed samples at varied section thickness

Generally, microstructures of the unetched and etched samples with section thickness of 10 mm, 30 mm and 85 mm at 0.05 wt.% Cu, 0.85 wt.% Cu and 1.35 wt.% Cu reveal traces of carbide in relative amount, which may be attributed to varied quantity of nickel. This is because nickel is a known good graphitizer, which suppresses carbide formation in Fe-C system by reducing carbon content in the eutectic and increasing the interval between austenite-graphite and austenite-cementite (Valek et al., 2012; Dwight, 1943) [41, 12]. And the fewer traces of carbide observed with 10 mm section thickness samples at the varied percent copper addition may be due to carbide suppression that resulted from high cooling rate (Haji and Husse, 2017) [14]. Also, attributable to nodule count and nodularity of the samples (Table 4) is cooling rate differential. And the more nodule counts and nodularity of 10 mm section thickness samples as compared to the 30 mm section and 85 mm thickness and 85 mm section thickness samples respectively resulted from faster cooling of the former (Gorny and Iyrala, 2012) [13].

Also, high nodularity (improved spherical graphite nodules) that are uniformly distributed with random orientation within ferrite-pearlite matrix (Plates a-c) with 10 mm section thickness samples at the varied percent copper addition of the varied copper addition resulted from fast cooling. In congruence, Haji and Husse, (2017) [14] have shown that

Hence, thin section regions are characterized by high nodularity. Conversely, the large graphite nodules, characterizing the revealed 30 mm and 85 mm section thickness samples correspondingly at the varied percent copper addition (Table 4) could be attributed to relative slow cooling rates. In agreement with Haji and Husse. (2017) [14], attributed the large/coarse graphite nodules, characterizing thick section to due to slow cooling. Decrease in nodule counts and increase in nodularity of the copper alloyed samples relative to the control samples (Table) at the constant section thickness (10 mm, 30 mm and 85 mm) (refer to Table 4) is indicative of the significance of copper on DI structure. And the increase in volume fraction of pearlite formation in the range of 0.05% -0.85wt.%Cu as compared to 0.85-1.35wt.%Cu have further shown that volume fraction of the DI phases, including comprising predominantly of ferrite and pearlite, and carbide phases were influenced differently by copper. Generally, fast cooling is associated with pearlite formation and slow cooling with ferrite formation, and as cooling increases, fraction of pearlite increase (Zou and Nakea, 2014) [22]. Therefore, the observed decrease in carbide phase precipitation with increasing cooling rate may be due to increased pearlite phase, which is in agreement with Collin-Garua et al, (2020) [10] who attributed decrease in carbide phase precipitation at fast cooling to increase in qualitative value of carbide phase in pearlite.

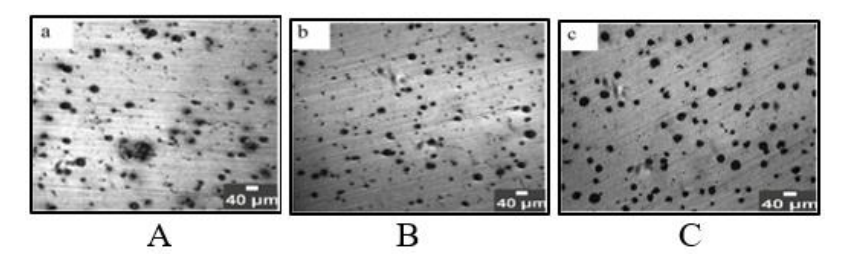
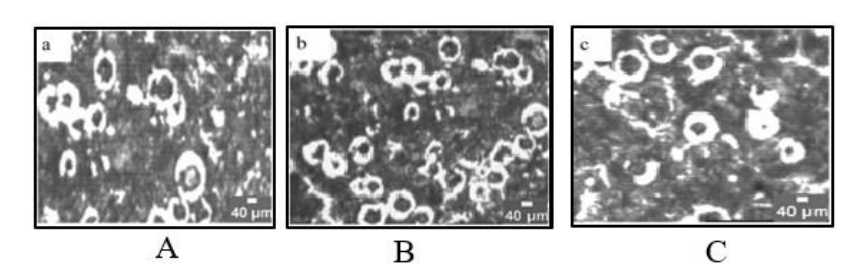
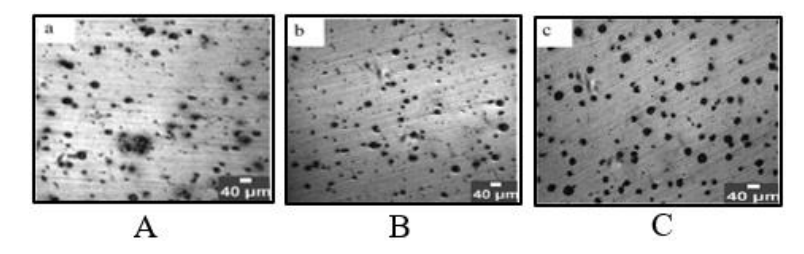


Plate 3: (a-c). Microstructures of the unetched 0.05wt.%Cu alloyed ductile iron with section thickness (a) 10 mm, (b) 35 mm and (c) 85 mm respectively



Plates 4(a-c): Microstructures of 0.05% Copper ductile iron with section thickness (a)10 mm, (b) 35 mm and (c) 85 mm respectively, etched in 3% nital solution



Plates 5(a-c): Un etched microstructures of 0.85% Copper ductile iron with section thickness (a)10mm, (b) 35mm and (c) 85mm respectively

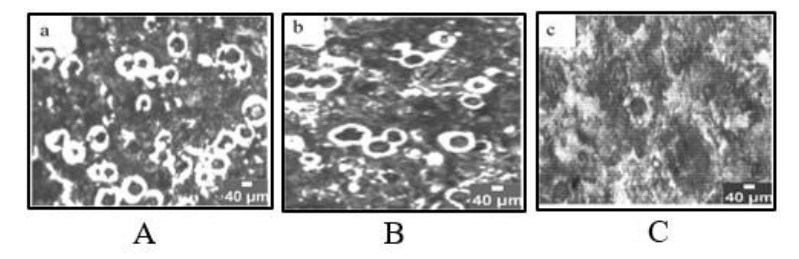


Plate 6 (a-c): Microstructures of 0.85% copper ductile iron with section thickness (a)10 mm, (b) 35 mm and (c) 85 mm respectively, etched in 3% nital solution

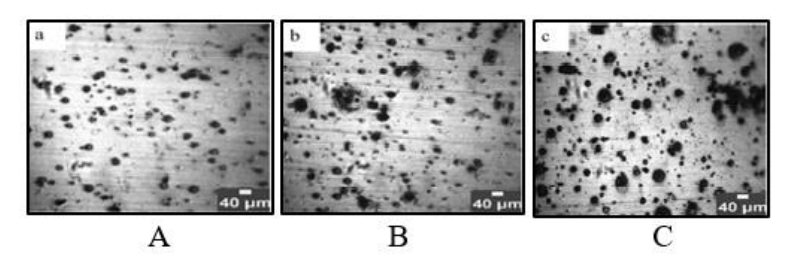


Plate7 (a-c): Un etched microstructures of 1.35% Copper ductile iron with section thickness (a)10 mm, (b) 35 mm and (c) 85 mm respectively

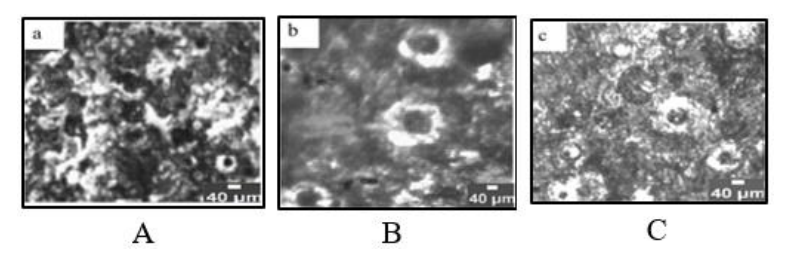


Plate 8 (a-c): Microstructures of 1.35% copper ductile iron with section thickness (a)10 mm, (b) 35 mm and (c) 85 mm respectively, etched in 3% nital solution

Table 4: Nodule count, nodularity, ferrite and pearlite volume fraction and carbide phase of the samples

Description	Section Thickness (mm)	Nodule count /(mm²)	Nodularity (%)	Volume fraction of ferrite (%)	Volume fraction of pearlite (%)	Carbide phase (%)
Control	10	201	85	53.67	46.33	11.80
Control	30	182	81	50.89	49.11	7.75
Control	85	160	77	48.68	51.32	5.45
0.05wt. % Cu	10	189	90	23.68	76.32	14.52
0.30 wt. %Cu	10	179	95	22. 11	77.89	16.02
0.85% wt. Cu	10	126	99	23.63	76.37	12.50
0.05wt. % Cu	30	172	87	23.32	76.68	16.02
0.30 wt. %Cu	30	139	92	21.29	78.71	9.67
0.85% wt. Cu	30	119	95	22.16	80.60	9.22
0.05wt. % Cu	85	129	84	19.08	80.92	7.92
0.30 wt. %Cu	85	112	89	19.40	80.60	9.67
0.85% wt. Cu	85	93	91	20.43	79.57	7.19

3.4 Mechanical properties

3.4.1 Tensile properties

In general, improved UTS and YS properties (Figs. 4a-b) of the copper alloyed samples as compared to the control was due to graphitization effect of copper (Hsu and Lin, 2011, Millis, 1985) ^[16]. And the superior UTS and YS values of the 10mm section thickness sample relative to the corresponding 35 mm and 85 mm section thickness samples could be

attributed to increased nodule count and good nodularity/spheroicity that resulted from high cooling rate (Haji and Husse, 2017; Gorny and Iyrala, 2012) [14,13]. And the presence of more volume fraction of pearlite was contributory (Behnam *et al.*, 2010) [7]. Improved ductility shown by 0.05wt.%Cu sample with section thickness of 85 mm relative to 0.85wt.%Cu sample with section thickness of 10 mm (Fig. 4c) was due to the large-grained phases that characterized the former. This is because fine grained phases, which are due to fast cooling are associate with decreased ductility, and large grained phases, which are due to slow cooling are associated with increased ductility ((Haji and Husse, 2017; Gorny and

Iyrala, 2012; Chakrabarti, 2005) [14, 13, 8]. And low ductility of 0.85wt.% Cu sample with section thickness of 10 mm may be hinged on relative deviation of graphite shape from the ideal spherical shape that resulted from fast cooling, and the presence of phase defects such as of flake graphite, crab graphite, vermicular graphite, exploded graphite and floated graphite (Bahubali and Vasudev, 2013; Allan, 2012) [1, 6]. The improved ductility of the control sample over the alloyed sample resulted from more volume fraction of ferrite. This is because ferrite is a softer phase, characterized by higher ductility, but lower yield strength than pearlite (Zou and Nakea, 2014) [22].

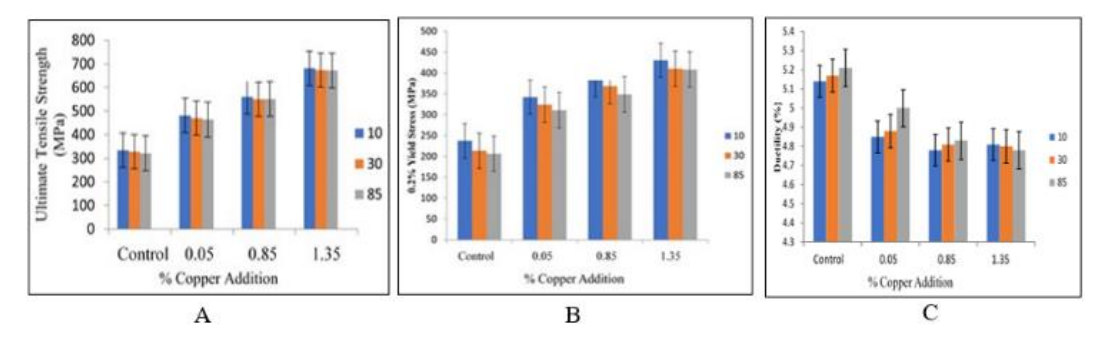


Fig 4: Tensile characteristics of the samples (a) ultimate tensile strength (b) yield strength and (c) ductility of the samples

3.4.2 Hardness property

Hardness property of the control sample is relative low as compared to 0.05 wt. %Cu., 0.05 wt. %Cu and 0.05 wt. %Cu samples correspondingly at that of the alloyed samples with at all the corresponding all section thickness (10 mm, 30 mm, 85 mm) (refer to Fig. 5), which be attributed to pearlite phase stabilization that resulted from synergistic effect of copper and cooling conditions (Tsuijikaiva, 2011) [20]. And decrease in hardness characteristics with increasing section thickness was due large - grained phases that resulted from decreasing cooling condition (Behnam *et al.*, 2010; Sahu *et al.*, 2014) [7, 18]

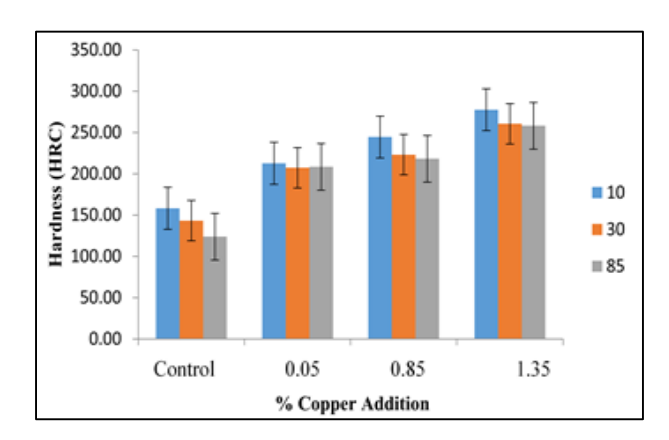


Fig 5: Hardness characteristics of the samples

3.4.3. Impact energy

The superior impact behavior of the control sample with section thickness (10 mm, 30 mm and 85 mm) over the corresponding 0.05 wt. % Cu., 0.85 wt. % Cu and 1.35 wt. % Cu samples was due to more volume fraction of pearlite phase that was accounted for by fast cooling that resulted from copper addition (Tsuijikaiva, 2011; Hsu and Lin, 2011) [20,16]. While the increasingly decrease in impact energy of the copper alloyed samples with increasing copper addition (0.05 wt. % Cu., 0.85 wt. % Cu and 1.35 wt. % Cu) was due to

increased deviation from spheriocity that resulted from fast cooling effect of copper (Hsu and Lin, 2011; Collin-Garua *et al.*, 2020; Dwight, 1943) [10, 12, 16]. Also, palpability of increased inclusion and defects with increased copper addition may be contributory.

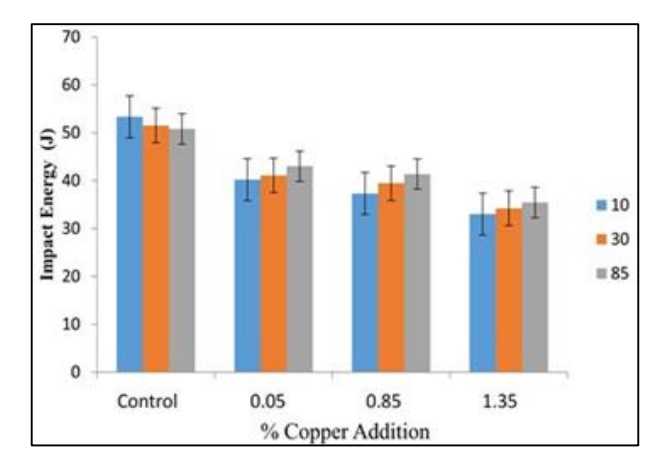


Fig 6: Impact energy characteristics of the samples

4. Conclusions

Based on the results, the following conclusions were drawn:

- 1. The control and copper alloyed samples are comprised majorly of silicon and other elements
- discribing the control (unetched) samples were comprised of homogeneously distributed spheroidal graphite in pearlitic-ferritic matrix, while microstructures of the control (etched) samples were characterized by graphite nodule of different sizes and spacing in pearlitic-ferritic matrix. Microstructures of the unetched and etched samples with section thickness of 10 mm, 30 mm and 85 mm at 0.05 wt.% Cu, 0.85 wt.% Cu and 1.35 wt.% Cu are characterized by traces of carbide in relative quantities, which decreased with increased copper addition. And the thinner is section thickness of 0.05 wt.% Cu, 0.85 wt.% Cu and 1.35 wt.% Samples, the more

- are nodule counts and nodularity. Converse was the case for thick section thickness samples.
- 3. Tensile characteristics (UTS and YS) of the copper alloyed samples were improved over the control samples at the corresponding section thickness of the samples. However, ductility (%E) of the control samples were superior to the copper alloyed samples with increasing proportion of copper addition.
- 4. Hardness characteristics of the control sample is comparatively 1 to the copper alloyed samples of corresponding section thickness.
- Impact energy characteristic of the control sample is high relative to the alloyed samples of corresponding section thickness.

5. References

- 1. Allan V. Microstructure and mechanical properties of austempered ductile iron. Internal Journal of Engineering; 2012;53-57.
- American Standard for Testing and Measurement E3-11.
 Standard guide for preparation of metallographic specimens. ASTM International; 2011. West Conshohocken. Available from: www.astm.org
- 3. American Standard for Testing and Measurement E384-11. Standard test method for microindentation hardness of materials. ASTM International; 2011. West Conshohocken. Available from: www.astm.org
- American Standard for Testing and Measurement E8-04.
 Standard test methods for tension testing of metallic materials. ASTM International; 2008. West Conshohocken. Available from: www.astm.org
- 5. American Standard for Testing and Measurement A327. Standard test methods for impact testing of cast irons. ASTM International; 2008. West Conshohocken. Available from: www.astm.org
- 6. Bahubali BS, Vasudev DS. Effect of inoculation on microstructure and mechanical properties of ductile iron. Journal of Mechanical and Civil Engineering. 2013;5(2):17-23.
- 7. Behnam MMJ, Davami P, Varahram N. Effect of cooling rate on microstructure and mechanical properties of grey cast iron. Materials Science and Engineering. 2010;A528(2):583-588.
- 8. Chakrabarti AK. Casting technology and cast alloys. New Delhi: PHI Private Limited; 2005;136.
- Choi JO, Kim JY, Choi CO, Kim JK, Rohatgi PK. Effect of rare earth element on microstructure formation and mechanical properties of thin wall ductile iron castings. Materials Science and Engineering A. 2004;383:323-333.
- Collin-Garua E, Crux-Ramirex A, Sanchez-Alvarado RG, Gutierreg-Perez VH, Reyes-Castellanous G. Nodule count effect on microstructure and mechanical properties of hypo-eutectic austempered ductile iron alloyed with nickel. Journal of Mining and Metallurgy. 2020;57(1):115-124.
- 11. Das AK, Dhal JP, Panda RK, Mishra SC, Sen S. Effect of alloying elements and processing parameters on mechanical properties of austempered ductile iron. Journal of Materials and Metallurgical Engineering. 2013;3(1):8-16.
- 12. Dwight M. Cast iron with spherical graphite. International Nickel Company Research Laboratory. 11th edition; 1943;22.

- 13. Gorny M, Iyrala E. Effect of cooling rate on microstructure and mechanical properties of thin-walled ductile iron casting. Journal of Materials Engineering. 2012;22:3000-305.
- 14. Haji MM, Husse F. Effect of cooling rate on the graphite nodule count and size distribution in nodular cast iron. Material Science Forum. 2017;925:45-53.
- Harvey JN, Noble GA. Inoculation of cast irons- An Overview. Tennant Metallurgical Group Ltd, Chesterfield, United Kingdom. 55th Indian Foundry Congress; 2007.
- Hsu CH, Lin KT. A study on microstructure and toughness of copper alloyed and austempered ductile irons. Materials Science and Engineering A. 2011;528:5706-5712. doi:10.1016/j.msea.2011.04.035.
- 17. Millis KD. Ductile iron data for design. 2nd edition. Ohio: Publication of Ductile Iron Society; 1985;250. New Delhi: Dhampart Rai Publications.
- 18. Sahu S, Bhat MN, Kumar A, Pratik A, Kumar A. Effect of section thickness on the microstructure and hardness of grey cast iron (A Simulation Study). International Journal of Engineering Research and Technology. 2014;3(7):35-40.
- 19. Skjegstad NT, Skaland T. Inoculation of grey and ductile iron. Elkem, Norway; 1996;4-15.
- 20. Tsuijikaiva M. Pearlite stabilization by copper on ductile cast iron. Key Engineering Materials and Technology. 2011;457:151-156.
- 21. Valek T, Simon P, Strilkova L. The composition of selected methods of cast iron spheroidisation in industrial conditions. Archives of Foundry Engineering. 2012;12(2):89-92.
- 22. Zou Y, Nakea H. Influence of boron on ferrite formation in copper added spheroidal graphite cast iron. Journal of China Foundry. 2014;11(4):375-381.